



Feasibility of Formation of $\text{Ge}_{1-x-y}\text{Si}_x\text{Sn}_y$ Layers With High Sn Concentration via Ion Implantation

Randall L. Holliday, Joshua M. Young, Satyabrata Singh, Floyd D. McDaniel* and Bibhudutta Rout*

Ion Beam Modification and Analysis Laboratory, Department of Physics, University of North Texas, Denton, Texas-76203, USA

*Email: mcdaniel@unt.edu; bibhu@unt.edu

ARTICLE INFORMATION

Received: October 10, 2019
Accepted: January 20, 2020
Published online: February 28, 2020

Keywords:

Photovoltaic cells, Ion implantation, Depth profile, Dynamic simulations



DOI: [10.15415/jnp.2020.72006](https://doi.org/10.15415/jnp.2020.72006)

ABSTRACT

By increasing the Sn concentration in $\text{Ge}_{1-y}\text{Sn}_y$ and $\text{Ge}_{1-x-y}\text{Si}_x\text{Sn}_y$ systems, these materials can be tuned from indirect to direct bandgap along with increasing electronic and photonic properties. Efforts have been made to synthesize Sn-Ge and Ge-Si-Sn structures and layers to produce lower energy direct-band gap materials. Due to low solid solubility of Sn in Ge and Si-Ge layers, high concentrations of Sn are not achieved by traditional synthesis processes such as chemical vapor deposition or molecular beam epitaxy. Implantation of Sn into Si-Ge systems, followed by rapid thermal annealing or pulse laser annealing, is shown to be an attractive technique for increasing Sn concentration, which can increase efficiencies in photovoltaic applications. In this paper, dynamic ion-solid simulation results are presented. Simulations were performed to determine optimal beam energy, implantation order, and fluence for a multi-step, ion-implantation based synthesis process.

1. Introduction

Direct bandgap reduction of Ge has been a topic of research for years. The most common way to engineer this has been to alloy Ge with Sn due to its lower band gap energy. One issue with this method is the decreasing in structural quality of the alloy at high Sn ($y > 0.12$) concentrations due to increased lasing threshold [1]. Another key problem with this approach is the low thermal stability of the binary $\text{Ge}_{1-y}\text{Sn}_y$ system as Sn concentrations increase above $y > 0.02$. In contrast to this, $\text{Ge}_{1-x-y}\text{Si}_x\text{Sn}_y$ offers a more stable alternative due to its larger mixing entropy [2]. Additionally, $\text{Ge}_{1-x-y}\text{Si}_x\text{Sn}_y$ ternary systems offer the ability to independently adjust both band gap and lattice constant such that, for a set lattice constant, band gaps can differ by more than 0.2 eV. This feature can prove vital in the development of devices from multicolor detectors to multi-junction photovoltaic cells, and through the decoupling of strain and band gap engineering, entirely new devices can be devised, ranging from conduction band quantum cascade lasers to solar cells [3]. In accordance with theoretical predictions, high Sn concentrations in this ternary system are associated with a significant enhancement of electronic and photonic properties, through the increase of direct bandgap emission [4]. Previously, Tran *et al.*, have reported synthesis of high quality $\text{Ge}_{1-x}\text{Sn}_x$ alloy with up to 6.2 atm% of Sn via implantation of 100 keV Sn into Ge substrate and subsequent pulse laser annealing [5]. However,

high Sn concentrations for this system are notoriously difficult to develop due to low solid solubility (a result of the aforementioned thermal instability [1]) of Sn in Si-Ge layers hindering traditional growth methods. In response to this problem, this paper will outline a multi-step ion-implantation process at various boundary conditions to synthesize research quality $\text{Ge}_{1-x-y}\text{Si}_x\text{Sn}_y$ samples, which has been a largely unexplored option up to this point.

Ion implantation remains a staple in the fabrication of semiconductor devices and in materials science research. By accelerating an ion of an element at low temperatures into a solid target, physical, chemical, and electrical properties can be altered. Due to the ballistic nature of the implantation process, amorphousness is expected at the implanted layer. This level of defects is of course, not ideal in many applications, thus necessitating an annealing process directly after implantation occurs to “restore lattice order”. How long and at what temperature annealing is done is a function of what ion was implanted, at what fluence, and at what energy.

2. Experimental

The end goal of these ion-solid interaction simulations are experimental ion implantation applications at the Ion Beam Modification and Analysis Laboratory (IBMAL) at the University of North Texas (UNT). Figure 1 shows the main laboratory of IBMAL [6].

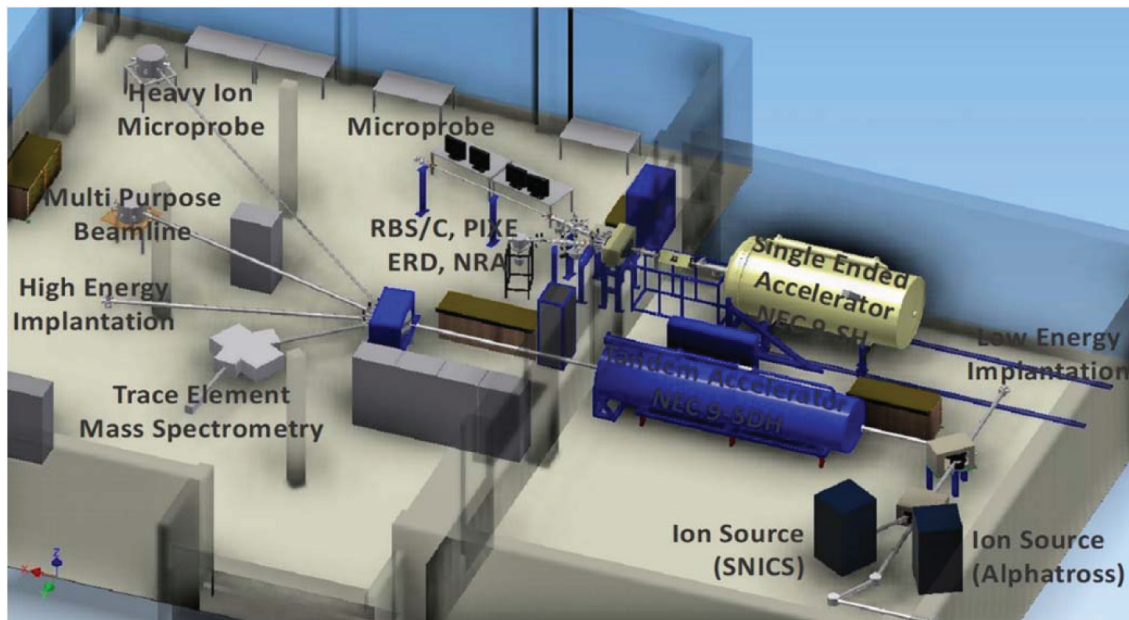


Figure 1: Ion Beam Modification and Analysis Laboratory (IBMAL) at the University of North Texas (UNT). The figure shows two of the particle accelerators, a National Electrostatic Corporation (NEC) Model 9-SDH-2 Tandem Accelerator and a NEC Model 9-SH Single-Ended Accelerator. Also shown are a number of the ion beam lines and their research function(s). The Low-Energy Ion Implantation Beam Line is located on the right-hand side of the two particle accelerators in the figure.

On the right-hand side of the figure are two of the particle accelerators in IBMAL. The lower one is a National Electrostatic Corporation (NEC) Model 9-SDH-2 Tandem Accelerator with a maximum terminal voltage (TV) of 3 MV, which can produce almost any ion in the Periodic Table at particle energies from 300 keV to 10s of MeV in different charge states. Ions produced by the Tandem Accelerator inject into: (1) the Trace Element Accelerator Mass Spectrometry Beam Line for high-sensitivity trace element analysis, (2) the High-Energy Ion Implantation Beam Line, (3) the Multi-Purpose Beam Line for routine sample analysis by Rutherford Backscattering spectrometry and Channeling (RBS/C), Particle-Induced X-Ray Emission (PIXE), Nuclear Reaction Analysis (NRA), and Elastic

Recoil Detection (ERD), and (4) a Heavy-Ion Microprobe Beam Line.

The upper accelerator is an NEC Model 9-SH Single-Ended Accelerator with a TV of 3 MV, which can produce positive ions from any gas substance at energies from 300 keV to 3 MeV. Ions, produced by the Single-Ended Accelerator, are injected into: (1) a Microprobe Beam Line, (2) a Multi-Purpose Beam Line for routine sample analysis by RBS/C, PIXE, NRA, and ERD, and (3) an Ion Implantation/irradiation Beam Line.

For this work, ions are produced by the Source of Negative Ions by Cesium Sputtering (SNICS) or Alphatrossion sources and may be injected directly into the low energy beam line after magnetic momentum/charge (mv/q) analysis

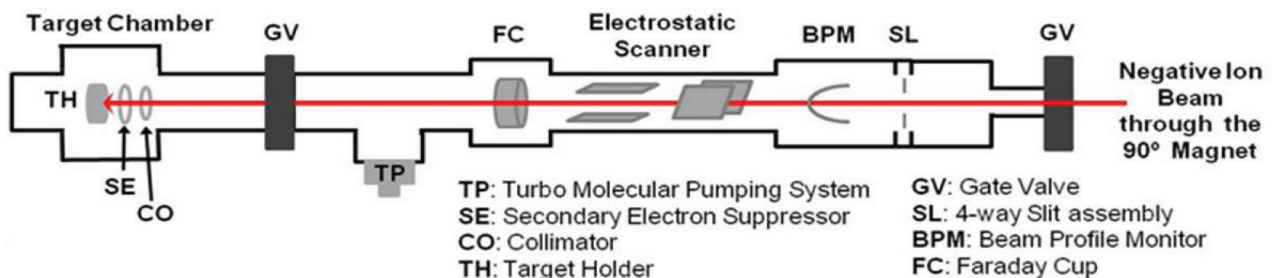


Figure 2: Essentially any ion in periodic table can be produced from the SNICS sputter ion source or the Alphatrossion ion source and uniformly implanted with fluences of 10^{12} to 10^{17} / cm^2 and ion energies of 20-80 keV over an area of 2.5 cm in diameter.

by the 30° magnet from the 9-SDH-2 tandem accelerator. Ion energies can be varied from 20-80 keV. Figure 2 is a schematic of the Low-Energy Ion Implantation Beam Line and shows the beam profile monitor and electrostatic raster scanner to uniformly-implant the ions of interest. Also shown are the Collimators (CO), Secondary Electron Suppressor (SE), and the Target Holder (TH).

3. Simulation Methods

SDTRIMSP is a dynamic version of the popular TRIM.SP code [7]. Where TRIM.SP strictly follows the central limit theorem, such that each particle is considered a possible state rather than a physical entity, SDTRIMSP

allows the target surface to change as a function of the imparted fluence. This allows the surface sputtering of the implanted target to be included in all subsequent histories, thus allowing for far greater accuracy in low energy, high fluence ion implantation scenarios. Depth profiles for various fluence and energy combinations were developed using the SDTRIMSP (version 5.00) package [8] as a means of effectively optimizing a synthesizing process. For comparison to traditional TRIM [9] simulations, Table 1 below details light ion implantation vs heavy ion implantation using TRIM and SDTRIMSP for 50 keV ions implanted at a 7° tilt angle with the normal to the surface to reduce ion channeling. The implantations were simulated for Si substrates.

Table 1: Comparison of TRIM [9] and SDTRIMSP [8] simulations for a range of ion masses from H to Au at 50 keV implant energy and at 7° tilt from the surface normal to prevent accidental channeling of the ions.

Ion	Static Code		Utilizing the Dynamic Simulation Code- SDTRIMSP			
	TRIM R _p (nm)	Mean projected range (nm) (for 1×10 ¹⁷ ions/cm ²)	Mean projected range (nm) (for 2×10 ¹⁷ ions/cm ²)	Total target atoms Sputtering Yield/ion	Implanted ion Sputtering Yield/ (2×10 ¹⁷ ions/cm ²)	Si Sputtering Yield/ (2×10 ¹⁷ ions/cm ²)
H	454.2	506.31	508.6	0	0	1.86×10 ¹⁵
He	413.1	418.63	421.79	0.02	7×10 ¹²	3.27×10 ¹⁵
C	151	151.34	160.84	0.223	4.66×10 ¹⁴	4.55×10 ¹⁶
Si	72.91	79.54	79.16	0.94	1.31×10 ¹⁶	1.75×10 ¹⁷
Fe	46	43.11	41.2	2.25	9.55×10 ¹⁶	3.47×10 ¹⁷
Ag	33.2	30.3	27.1	4.06	1.58×10 ¹⁷	6.53×10 ¹⁷
Au	29.81	21.79	20.96	5.46	1.72×10 ¹⁷	9.19×10 ¹⁷

4. Results and Discussion

Simulations were performed in order to determine optimal ion beam energy, fluence, and implantation order. Figures 3-7 below outline this process.

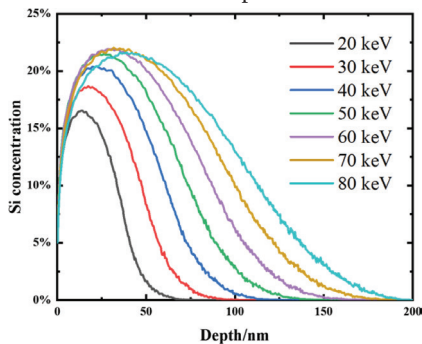


Figure 3: Simulated distribution of Si implanted into Ge at various energies from 20-80 keV with a constant fluence of 1.5×10¹⁷ atoms cm⁻².

Figure 3 outlines all energy variations achievable using the IBMAL low energy beam line. As can be seen, peak concentration is reached at 70 keV, with maximal distribution being achieved at 80 keV.

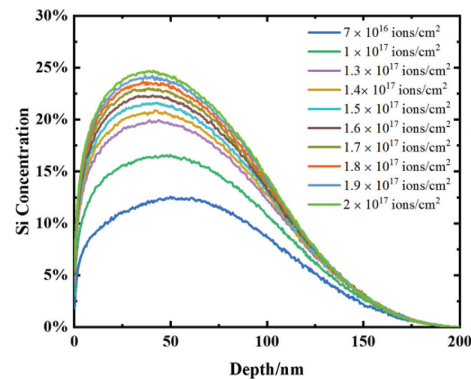


Figure 4: Simulated distribution of Si into Ge at 80 keV for various fluences.

Due to the increased implanted total, an 80 keV energy beam implantation of Si into a pure Ge sample provides the best base for subsequent steps in this process. At this energy, the Si implant (with an ion fluence of 1.5×10^{17} atoms cm^{-2}) depth profile peaks around 45 nm with an elemental concentration $\sim 23\%$. The ion range is seen up to about 200 nm.

Figure 4 outlines a range of potential beam fluences for the 80 keV Si implantation. While distribution patterns are not affected by this variable, there is a direct correlation with total Si concentration as fluence is increased. This level of increase decays as fluence rises, asymptotically approaching its peak (saturation) of $\sim 25\%$. Due to this asymptotic nature, a beam fluence of 2×10^{17} atoms cm^{-2} was decided as the optimal fluence for the first step of this double implantation process.

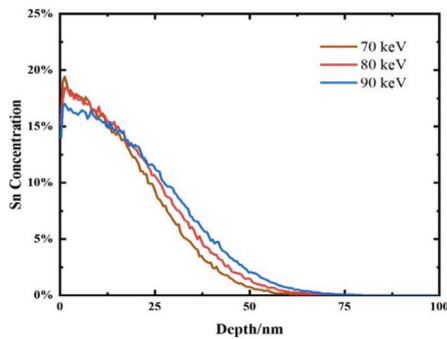


Figure 5: Simulated distribution of Sn onto GeSi surface at various energies and constant fluence. The Sn was implanted at a fluence of 1.5×10^{17} atoms cm^{-2} .

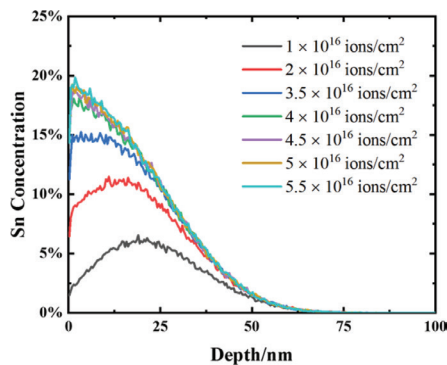


Figure 6: Simulated distribution of Sn into GeSi at 80 keV for various fluences.

Using the first implantation outlined by Figures 3 and 4 as the implanting surface (80 keV Si implanted into Ge at a fluence of 2×10^{17} atoms cm^{-2}), Figure 5 outlines all energy variations achievable using the low energy beam line at IBMAL for the implantation of Sn. Similar to the first

implantation, a beam energy of 80 keV proved to be optimal under the set boundary conditions.

Figure 6 shows the final step in the development of our double implantation recipe. Using an 80 keV beam energy, as determined in Figure 5, various fluences were tested to determine the optimal Sn concentration. As was the case in the first implantation, an asymptotic value was determined, and a fluence of 5×10^{16} atoms cm^{-2} was determined to be an optimal fluence for the implantation of Sn onto our previously implanted GeSi surface.

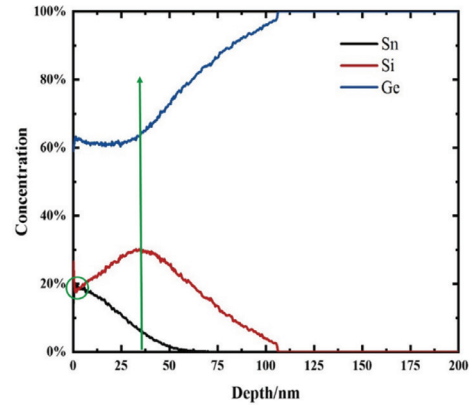


Figure 7: 80 keV Sn implantation at fluence of 5×10^{16} atoms cm^{-2} implanted into 80 keV, 2×10^{17} atoms cm^{-2} , Si implanted Ge surface.

Figure 7 shows the culmination of the process developed using Figures 3-6. From these simulations, it was determined that optimal low beam energy for the saturation of Si into Ge and for the saturation of Sn into the subsequent GeSi surface is 80 keV, saturation fluence for Si into Ge at 80 keV beam energy is 2×10^{17} atoms cm^{-2} , and saturation fluence for Sn into this GeSi surface at 80 keV beam energy is 5×10^{16} atoms cm^{-2} . The concentrations of Sn, Si, and Ge as a function of depth in the Ge materials is shown in Figure 7. At the green line (30 nm depth), the ratio of Si:Sn is 3.7, which presents a lattice matched alloy with the Ge substrate [10, 11]. This strain-free layer is more stable structure than $\text{Ge}_{1-y}\text{Sn}_y$ structure and shows enhanced optical properties. Also, study shows that the presence of higher Sn content in the $\text{Ge}_{1-x-y}\text{Si}_x\text{Sn}_y$ makes the system more direct bandgap with lower bandgaps and emission of PL signal at lower energy suitable for longer wave length transmission [1]. In fact, in the region up to 4 nm from the surface (Green Circle) the concentration of Sn is more than Si. This region, which is much better for PL emission, enables transitions from direct bandgaps beyond 1550 nm, which is better for telecommunication. Also, if the increase in Si is more than 20%, the band gap begins to increase and become indirect.

With this information, this simulated multi-step implantation process can be experimentally tested, thus expediting the development of this important composite electronic material.

Conclusions

Ion beam implantation remains a staple in the synthesizing of research quality materials. By allowing multiple ratios of materials to be present in a single sample, both time and resources can be preserved in the case study of materials. Optimal conditions for this particular ternary system are subject to small changes due to the requirements of individual experiments performed in the future. This work has provided a foundation for future research into this incredibly versatile group IV semiconductor at IBMAL. Further simulations will be performed to explore the implantation of Sn onto a Ge implanted Si sample to further optimize the synthesis process.

Acknowledgements

The authors would like to thank Dr. Andreas Mutzke from the Max-Planck-Institute of Plasmaphysics, Germany, for providing the latest version of the SDTrimSP simulation code.

References

- [1] P. Zaumseil, Y. Hou, M. A. Schubert, N. V. D. Driesch, D. Stange, D. Rainko, M. Virgilio, D. Buca, G. Capellini., *APL Materials* **6**, 076108 (2018).
<https://doi.org/10.1063/1.5036728>
- [2] C. Xu, L. Jiang, J. Kouvetakis, J. Menéndez, *Appl. Phys. Lett.* **103**, 072111 (2013).
<https://doi.org/10.1063/1.4818673>
- [3] John Kouvetakis, John Tolle, RadekRoucka, Vijay R. D'Costa, Yan-yan Fang, Andrew V. Chizmeshya, Jose Menendez., *ECS Trans.* **16**, 807 (2008).
<https://doi.org/10.1149/1.2986840>
- [4] D. Rainko, Z. Ikonc, N. Vukmirović, D. Stange, N. V. D. Driesch, D. Grützmacher & D. Buca, *Scientific Reports* **8**, 15557 (2018).
<https://doi.org/10.1038/s41598-018-33820-1>
- [5] T. T. Tran, D. Pastor, H. H. Gandhi, L. A. Smillie, A. J. Akey, M. J. Aziz and J. S. Williams, *Journal of Applied Physics* **119**, 183102 (2016).
<https://doi.org/10.1063/1.4948960>
- [6] B. Rout, M. S. Dhoubhadel, P. R. Poudel, V. C. Kummari, B. Pandey, N. T. Deoli, W. J. Lakshantha, S. J. Mulware, J. Baxley, J. E. Manuel, J. L. Pacheco, S. Szilasi, D. L. Weathers, T. Reinert, G. Glass, J. L. Duggan, F. D. McDaniel, IX International Symposium on Radiation Physics, Puebla, Mexico, April 14-17, 2013, *AIP Conference Proceedings* **1544**, 11 (2013).
<https://doi.org/10.1063/1.4813454>
- [7] A. Mutzke, R. Schneider, W. Eckstein, R. Dohmen, IPP Report 12/8 Garching, (2011).
- [8] W. J. Lakshantha, V. C. Kummari, T. Reinert, F. D. McDaniel, B. Rout, *Nucl. Inst. And Meth. B* **332**, 33 (2014).
<https://doi.org/10.1016/j.nimb.2014.02.024>
- [9] J. F. Ziegler, M. D. Ziegler and J. P. Biersack, *Nuclear Instruments and Methods in Physics* **268**, 1818 (2010).
<https://doi.org/10.1016/j.nimb.2010.02.091>
- [10] V. R. D'Costa, Y.-Y. Fang, J. Tolle, J. Kouvetakis and J. Menéndez, *Phys. Rev. Lett.* **102**, 107403 (2009).
<https://doi.org/10.1103/PhysRevLett.102.107403>
- [11] T. Yamaha, S. Shibayama, T. Asano, K. Kato, M. Sakashita, W. Takeuchi, O. Nakatsuka and S. Zaima, *Appl. Phys. Lett.* **108**, 061909 (2016).
<https://doi.org/10.1063/1.4941991>



Journal of Nuclear Physics, Material Sciences, Radiation and Applications

Chitkara University, Saraswati Kendra, SCO 160-161, Sector 9-C,
Chandigarh, 160009, India

Volume 7, Issue 2

February 2020

ISSN 2321-8649

Copyright: [© 2020 Floyd D. McDaniel et al.] This is an Open Access article published in Journal of Nuclear Physics, Material Sciences, Radiation and Applications (J. Nucl. Phy. Mat. Sci. Rad. A.) by Chitkara University Publications. It is published with a Creative Commons Attribution- CC-BY 4.0 International License. This license permits unrestricted use, distribution, and reproduction in any medium, provided the original author and source are credited.
